Integration of a Multimode Interference Coupler With a Corrugated Sidewall Bragg Grating in Planar Polymer Waveguides

Lin Zhu, Yanyi Huang, and Amnon Yariv

***Abstract*—We demonstrate the integration of a 3-dB multimode interference coupler with a corrugated sidewall Bragg grating in planar polymer waveguides by direct electron beam writing. Both transmission and reflection spectra of the Bragg grating are measured through this integrated device directly. We use the thermooptic effect to tune the integrated waveguide grating, achieving a tuning range of 6.2 nm and a bandwidth variation of 0.3 nm within a temperature change of 62 °C.**

***Index Terms*—Integrated optoelectronics, multimode interference (MMI) couplers, polymer gratings.**

I. Introduction

INTEGRATED optical devices have become important components for optical fiber communication systems. Polymer materials offer a very promising platform to fabricate integrated optical devices on a planar substrate, owing to the advantages of easy processing, mechanical flexibility, and potentially low production cost [1]. Polymer Bragg gratings have been fabricated by a variety of techniques such as photolithography (photochemical process) [2]–[4], oxygen plasma reactive ion etching (RIE) [5], [6], and direct electron beam writing [7], [8]. The photolithography technique requires photosensitive polymer materials. The relative refractive index modulation $\Delta n/n$ induced by a photochemical process is normally limited to around 10^{-4} – 10^{-3} [2]. Both plasma etching and direct electron beam writing can achieve a larger relative refractive index modulation $\Delta n/n$ of $\sim$0.001–0.1. RIE processing transfers a grating pattern from the top polymer layer to the core underneath. It increases the difficulty of obtaining accurate and smooth waveguide gratings. Direct electron beam writing provides high flexibility and minimal fabrication errors, but requires the electron beam sensitive polymer material with good optical properties. Previous work using direct electron beam writing mainly focused on surface relief gratings [7], [8]. Recently, we have applied direct electron beam writing to fabricate corrugated sidewall Bragg gratings in polymer waveguides and demonstrated multichannel passband filters based on a phase-shifted design [9].

It is highly desirable to integrate this on-chip sidewall grating with other planar optical components in polymer waveguides because the combination of Bragg gratings with optical couplers, Mach–Zehnder interferometers, and lasers has created many important multifunction devices, such as optical add–drop multiplexers (OADMs), optical switches/routers, and distributed feedback lasers [10]. Meanwhile, the direct electron beam writing technique offers the great advantage of eliminating alignment errors in the integration of planar grating structures with other device structures since all the patterns are written sequentially by a precisely controlled electron beam.

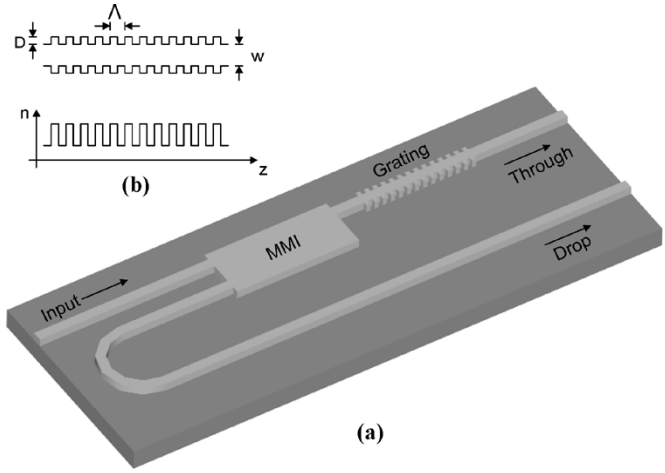

Fig. 1. Schematic diagrams of (a) the designed device structure of an integrated MMI with waveguide gratings in one arm and (b) the top view of corrugated sidewall waveguide gratings and the corresponding effective refractive index profile along the propagation direction.

In this letter, we use the polymer material to integrate a 3-dB multimode interference (MMI) coupler with a corrugated sidewall Bragg waveguide grating on an oxidized silicon substrate. The fabricated device realizes the function of an OADM filter and has a compact size. In addition, we take advantage of the large thermooptic coefficient dn/dT (refractive index change with temperature) of the polymer material to demonstrate tunability of the fabricated device.

II. Device Design and Fabrication

Fig. 1(a) shows the proposed device structure of an integrated MMI coupler with a waveguide grating. The reason we chose an MMI coupler is that it has a good fabrication parameter tolerance, does not require a small coupling gap as in evanescent couplers, and has a compact size [11]. Fig. 1(b) shows the top view of a corrugated sidewall Bragg grating and the corresponding effective refractive index profile along the propagation direction. This corrugated sidewall design is superior to a conventional buried

Manuscript received November 17, 2005; revised January 6, 2006. This work was supported by the National Science Foundation and Defense Advanced Research Projects Agency.

The authors are with the Department of Electrical Engineering and Department of Applied Physics, California Institute of Technology, Pasadena, CA 91125 USA.

Digital Object Identifier 10.1109/LPT.2006.871125

grating structure (surface relief grating) for the control of the effective index modulation [12], [13]. The device operation can be explained in the following way: An optical signal is launched through the input port at one end of the MMI coupler. Two images of the input signal will be symmetrically distributed at the other end of the coupler through the mode coupling. By integrating the waveguide grating in the output arm of the MMI coupler, the transmitted signal outside the grating bandwidth will pass the "through" port, while the signal within the grating bandwidth will be reflected back and taken out from the "drop" port.

To fabricate the device in Fig. 1(a), a 1.6-μm-thick layer of the negative electron beam resist SU-8 (Microchem) is first spun onto a silicon wafer with 5 μm of thermally grown silicon oxide, which serves as the lower cladding. Then, the MMI coupler and waveguide grating are directly patterned by electron beam exposure using a scanning electron microscope. As the waveguide core, the crosslinked SU-8 exhibits a relatively high refractive index ($n = 1.565$ at 1550 nm). The waveguide does not have an upper cladding. Finally, the sample is developed by propylene glycol monomethyl ether acetate and dried by nitrogen gas. The device end facets are formed by cleaving the silicon substrate.

III. Results and Discussions

It is important to obtain a 50/50 coupling ratio between two output arms of the MMI coupler in order to minimize transmission loss of the drop port [10]. Thus, we first fabricate a series of MMI couplers (without the waveguide grating) with different coupling lengths to obtain the optimal design. The width and height of the MMI couplers are 6 and 1.6 μm, respectively. During the measurement, since it is difficult to maintain exactly the same input coupling efficiency for different devices, we choose the power ratio between two output arms as the measure parameter. The input signal at wavelength of 1.55 μm is first transmitted through a polarization scrambler to obtain an average result among all polarization states. In Fig. 2(a), the solid line shows the experimental result of the power ratios between the two output arms with different MMI lengths, and the dashed line shows the corresponding numerical simulation result calculated by a beam propagation method (BPM). We achieve a good agreement between the experimental measurements and the theoretical calculations. Fig. 2(b) shows the BPM simulation result of the normalized power of two output ports with different MMI lengths. Comparing Fig. 2(a) and (b), we can find the optimal 3-dB coupling length, which provides not only the equally distributed intensities of two image fields but also the highest transmission intensity, is approximately 95 μm.

Given the optimum coupling length of 95 μm, we can fabricate the final device by integrating the waveguide grating in one arm of the MMI coupler. The grating has a waveguide width W of 1.5 μm, grating period Λ of 520 nm, and grating depth D of 500 nm. The grating length is 560 μm and the total device length is around 1.2 mm. In Fig. 3, the solid line represents the experimental result of the device frequency response spectra for both the drop [Fig. 3(a)] and through [Fig. 3(b)] ports, and the dashed line represents the corresponding numerical fitting based on a transmission matrix method. The transmission and reflection spectra are complementary to each other, indicating that

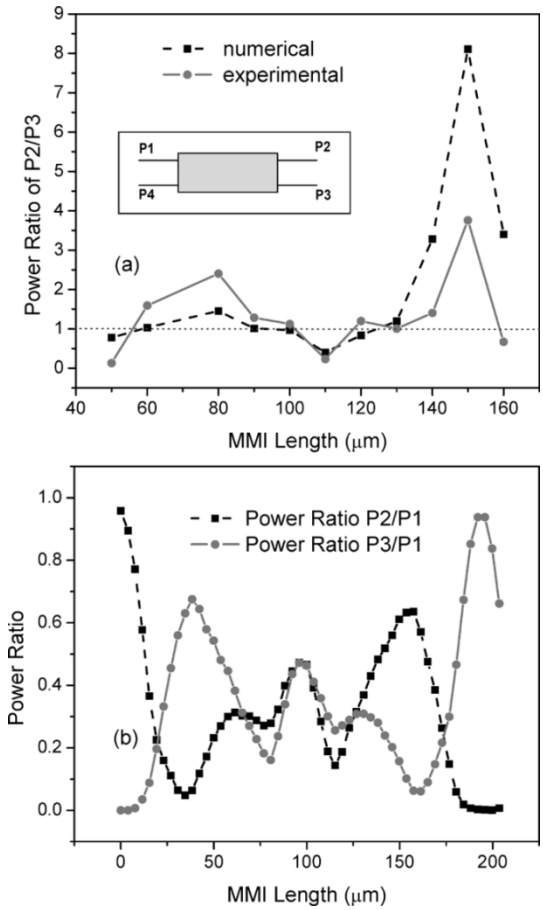

Fig. 2. (a) Dependence of the power ratio between Port 2 and Port 3 upon MMI length. Inset: the layout of the MMI coupler. Compared to Fig. 1, P1 is the input port, P2 is arranged to be integrated with gratings, P3 is added for the device characterization, and P4 is the drop port. (b) Dependence of the power ratio of P2/P1 and P3/P1 upon MMI length (simulation only). Experimental results and theoretical simulations achieve good agreement in (a), and the 3-dB coupling length is around 95 um.

the reflection signal from the sidewall Bragg grating has been coupled back through the MMI coupler. The wavelength-dependent loss observed within the central lobe of the drop port spectrum comes mainly from scattering loss. The central wavelength of the grating bandgap is around 1573.6 nm and the 3-dB bandwidth is about 2.9 nm. According to the numerical fittings, the measured spectra correspond to an effective index n_{eff} of 1.513 and grating index modulation Δn of 0.0047. The sidelobes present in the transmission spectra originate from the constant grating index modulation profile used for the fabricated device. Through the design of an appropriate apodization profile, i.e., varying the grating depth D along the propagation direction, the sidelobe amplitude can possibly be suppressed [12], [13].

The insertion loss is 11 dB at the through port off resonance (outside the grating bandwidth) and 18 dB at the drop port on resonance (inside the grating bandwidth). The insertion loss mainly comes from the propagation loss, coupler imaging loss, and fiber-to-device coupling loss. The radius of the curve in the device is around 100 um, so the bending loss for the drop port is expected to be less than 1 dB. Assuming the input and output coupling losses are the same for the through and drop ports, the propagation loss for the device is estimated about 22 dB/cm, which includes both material loss and scattering loss.

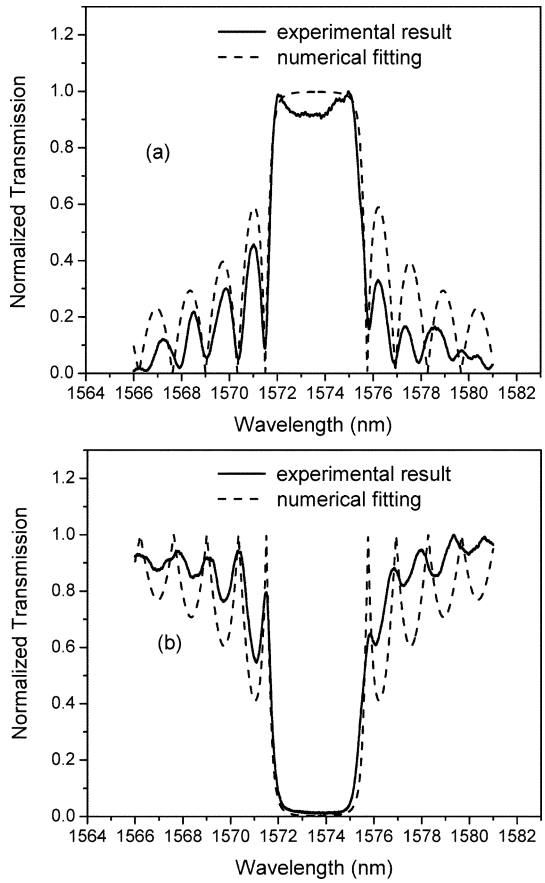

Fig. 3. Normalized frequency response spectra of the fabricated device, (a) drop port, (b) through port. The central wavelength of the spectra is 1573.6 nm and the 3-dB bandwidth is 2.9 nm.

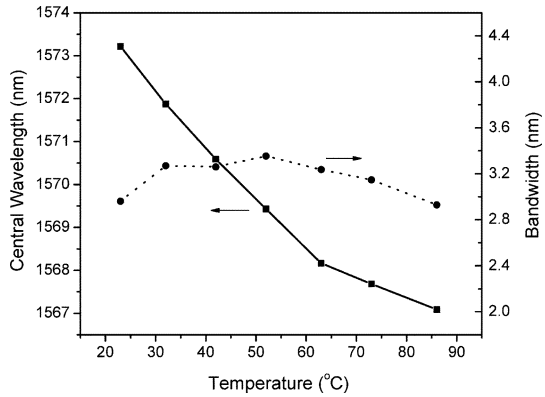

Fig. 4. Temperature dependence of the central wavelength and bandwidth of the grating spectrum response.

The device temperature is changed by directly heating the substrate after the chip is mounted on a micro heater. Fig. 4 shows the dependence of the central bandgap wavelength and bandwidth of the fabricated device transmission spectra on temperature. The central wavelength is blue shifted with the increase of the device temperature. From 24 °C to 86 °C, we observe a tuning range of 6.2 nm for the central wavelength. The corresponding average thermooptic coefficient of the polymer waveguide grating can be calculated as

$$\frac{dn}{dT} = \frac{m}{2\Lambda} \cdot \frac{\Delta\lambda}{\Delta T} = -9.6 \times 10^{-5} K^{-1}$$

where Λ is the period of the grating, m is the order of Bragg reflection, $\Delta\lambda$ is the change of the central wavelength, and $\Delta T\iota\sigma$ the change in device temperature. We find that the rate of change of the central wavelength is roughly constant from 20 °C to 60 °C, but decreases slightly when the device temperature is increased beyond 60 °C. This is probably due to the slight deformation of the polymer device at relatively high temperatures. As illustrated in Fig. 4, the temperature also affects the device bandwidth, causing it to vary within a range between 2.9 and 3.2 nm. This comes from the change of the waveguide core index, which also leads to the variation of index modulation of the grating.

IV. Conclusion

We have applied electron beam direct writing to demonstrate the fabrication of a polymeric 3-dB MMI coupler integrated with a uniform corrugated sidewall waveguide grating. The fabricated device functions as a broad-band OADM filter, with a nominal bandwidth of 2.9 nm. The thermooptic effect is used to tune the integrated device, achieving a tuning range of 6.2 nm and a bandwidth variation of 0.3 nm within a temperature change of 62 °C.

Acknowledgment

The authors would like to thank J. Choi, Dr W. Green, and J. Poon for helpful discussions.

References

[1] L. Eldada and L. W. Shaklette, "Advances in polymer integrated optics," *IEEE J. Sel. Topics Quantum Electron.*, vol. 6, no. 1, pp. 54–68, Jan./Feb. 2000.

[2] L. Eldada, S. Yin, C. Poga, C. Glass, R. Blomquist, and R. A. Norwood, "Integrated multichannel OADMs using polymer Bragg grating MZIs," *IEEE Photon. Technol. Lett.*, vol. 10, no. 10, pp. 1416–1418, Oct. 1998.

[3] L. Eldada, R. Blomquist, M. Maxfield, D. Pant, G. Boudoughian, C. Poga, and R. A. Norwood, "Thermooptic planar polymer Bragg grating OADMs with broad tuning range," *IEEE Photon. Technol. Lett.*, vol. 11, no. 4, pp. 448–450, Apr. 1999.

[4] W. C. Wang, M. Fisher, A. Yacoubian, and J. Menders, "Phase-shifted Bragg grating filters in polymer waveguides," *IEEE Photon. Technol. Lett.*, vol. 15, no. 4, pp. 548–550, Apr. 2003.

[5] M. C. Oh, M. H. Lee, J. H. Ahn, H. J. Lee, and S. G. Han, "Polymeric wavelength filters with polymer gratings," *Appl. Phys. Lett.*, vol. 72, pp. 1559–1561, 1998.

[6] M. C. Oh, H. J. Lee, M. H. Lee, J. H. Ahn, S. G. Han, and H. G. Kim, "Tunable wavelength filters with Bragg gratings in polymer waveguides," *Appl. Phys. Lett.*, vol. 73, pp. 2543–2546, 1998.

[7] M. C. Oh, S. Ura, T. Shhara, and H. Nishihar, "Integrated-optic focal-spot intensity modulator using electrooptic polymer waveguide," *J. Lightw. Technol.*, vol. 12, no. 9, pp. 1569–1576, Sep. 1994.

[8] W. H. Wong and E. Y. B. Pun, "Polymeric waveguide wavelength filters using electron-beam direct writing," *Appl. Phys. Lett.*, vol. 79, pp. 3576–3578, 2001.

[9] L. Zhu, Y. Huang, W. M. J. Green, and A. Yariv, "Polymeric multichannel bandpass filters in phase-shifted Bragg waveguide gratings by direct electron beam writing," *Opt. Express*, vol. 12, pp. 6372–6376, 2004.

[10] R. Kashyap, *Fiber Bragg Gratings*. New York: Academic, 1999.

[11] L. Soldano and E. Pennings, "Optical multi-mode interference devices based on self-imaging: Principles and applications," *J. Lightw. Technol.*, vol. 13, no. 4, pp. 1424–1432, Apr. 1997.

[12] T. Segawa, S. Matsuo, Y. Ohiso, T. Ishii, and H. Suzuki, "Apodised sampled grating using InGaAsP/InP deep-ridge waveguide with vertical-groove surface grating," *Electron. Lett.*, vol. 40, pp. 804–805, 2004.

[13] T. Segawa, S. Matsuo, Y. Ohiso, T. Ishii, Y. Shibata, and H. Suzuki, "Fast tunable optical filter using cascaded Mach–Zehnder interferometers with apodized sampled gratings," *IEEE Photon. Technol. Lett.*, vol. 17, no. 1, pp. 139–141, Jan. 2005.